# Ligand Fluxionality in Close-packed Rhodium Carbonyl Clusters

**Claudio Allevi, Brian T. Heaton,*† Claudio Seregni, and Luisella Strona**
*Chemical Laboratory, University of Kent, Canterbury CT2 7NH*
**Robin J. Goodfellow**
*Department of Inorganic Chemistry, The University, Bristol BS8 1TS*
**(The late) Paolo Chini**
*Istituto di Chimica dell'Università, Via G Venezian 21, 20133 Milano, Italy*
**Secondo Martinengo***
*Centro del CNR per lo Studio della Sintesi e Della Struttura dei Composti dei Metalli di Transizione, Via G Venezian 21, 20133 Milano, Italy*

A combination of variable-temperature, multinuclear n.m.r. studies ($^1$H, $^{13}$C, $^{103}$Rh, $^1$H-{$^{103}$Rh}, and $^{13}$C-{$^{103}$Rh}) has allowed the ligand (CO/H) migrations in $[Rh_{13}(CO)_{24}H_n]^{(5-n)-}$ ($n$ = 1—4) and $[Rh_{14}(CO)_{25}H_x]^{(4-x)-}$ ($x$ = 0 or 1) to be established. In both types of compound, interstitial H migration is found at room temperature with complete randomisation of carbonyls in the $Rh_{14}$ clusters and partial migration of carbonyls in the $Rh_{13}$ clusters; in neither case is there evidence for rearrangement of the metal polyhedron. At low temperatures (−90 °C), H migration still occurs in $[Rh_{14}(CO)_{25}H]^{3-}$ but not in $[Rh_{13}(CO)_{24}H_3]^{2-}$ and $[Rh_{13}(CO)_{24}H_2]^{3-}$ which have the same structural features as found in the solid state with the hydride ligands occupying pseudo-octahedral holes in the metal skeleton. All the values of $\delta(^{103}Rh)$ for the interstitial rhodium atoms are at significantly higher frequency than the values for the surface rhodium resonances and shift significantly to lower frequency with increasing interstitial hydride content.

The anions $[Rh_{13}(CO)_{24}H_n]^{(5-n)-}$ ($n$ = 1—4) provide a unique series of isostructural, multihydride clusters. They are all interconvertible by addition or removal of a proton and the mono-, di-, and tri-hydride derivatives have all been isolated as crystalline solids and examined by $X$-ray crystallography.[1-3] They have similar structures consisting of a hexagonal close-packed metal skeleton in which each surface rhodium is co-ordinated to one terminal and two edge-bridging carbonyls [Figure 1(*a*)]. The hydride ligands were not located in the $X$-ray studies but were suggested to be close to the metal square faces [$Rh^1Rh^3Rh^4Rh^5$, $Rh^6Rh^7Rh^{11}Rh^{12}$, and $Rh^8Rh^9Rh^{10}Rh^{12}$ in Figure 1(*a*) are progressively occupied for $n$ = 1, 2, and 3 respectively], which are situated below the pentagonal holes found on the surface of the carbonyl polyhedron. This is in agreement with the present n.m.r. data, see later.

The formation of $[Rh_{14}(CO)_{25}H_x]^{(4-x)-}$ ($x$ = 0 or 1)[4,5] and $[Rh_{15}(CO)_{27}]^{3-}$ [5] may be considered to result from similar electrophilic additions [equations (1) and (2)] to the same square faces of the $Rh_{13}$ cluster as shown schematically in Figure 1(*b*) and (*c*); in both cases, the actual structures can

$$[Rh_{13}(CO)_{24}H]^{4-} + [Rh(CO)_2(CH_3CN)_2]^+ \longrightarrow [Rh_{14}(CO)_{25}H]^{3-} + CO + 2CH_3CN \quad (1)$$

$$[Rh_{14}(CO)_{25}]^{4-} + [Rh(CO)_2(CH_3CN)_2]^+ \longrightarrow [Rh_{15}(CO)_{27}]^{3-} + 2CH_3CN \quad (2)$$

be derived from those in the scheme after a minimum reorganisation of the Rh–Rh bonds and the carbonyl polyhedron. Another schematic representation of $[Rh_{14}(CO)_{25}H_x]^{(4-x)-}$ ($x$ = 0 or 1), which emphasises the

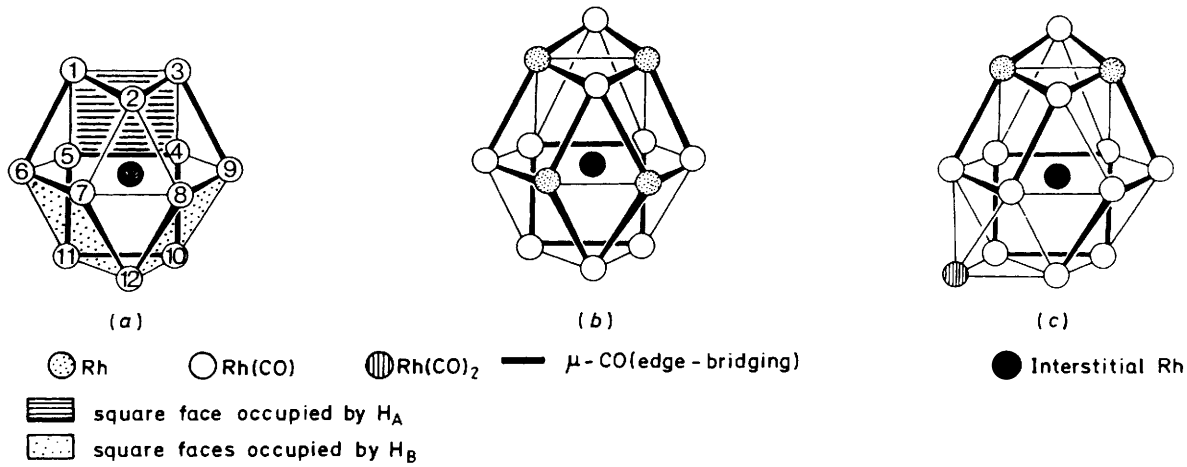


**Figure 1.** Schematic representation of a possible $Rh_{13} \longrightarrow Rh_{15}$ cluster growth pathway: (*a*) $[Rh_{13}(CO)_{24}H_n]^{(5-n)-}$ ($n$ = 1—4), (*b*) $[Rh_{14}(CO)_{25}H_x]^{(4-x)-}$ ($x$ = 0 or 1), (*c*) $[Rh_{15}(CO)_{27}]^{3-}$; $H_A$ and $H_B$ can be replaced by $Rh(CO)_z$ ($z$ = 1 or 2) in (*b*) and (*c*) respectively

† *Present address*: Department of Inorganic, Physical and Industrial Chemistry, P.O. Box 147, University of Liverpool, Liverpool L69 3BX.

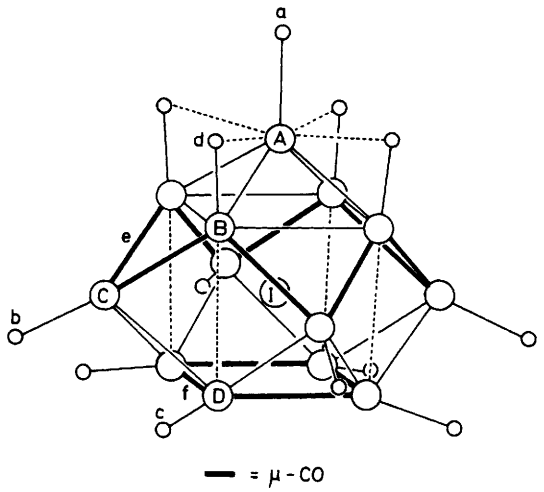


**Figure 2.** Schematic representation of the *X*-ray structure of $[Rh_{14}(CO)_{25}H_x]^{(4-x)-}$ ($x = 0$ or 1) illustrating the $C_{4v}$ symmetry

four-fold symmetry resulting from the carbonyl distribution, is shown in Figure 2. There is no information about the location of the hydride in the solid-state structure of the species with $x = 1$ and low-temperature n.m.r. data show it to be still fluxional. This fluxionality is shown to occur *via* interstitial site migrations and is similar to the behaviour of $[Rh_{13}(CO)_{24}H_n]^{(5-n)-}$ ($n = 1$—4) at higher temperatures. These two types of clusters are presently unique in providing examples of interstitial H migration which serve as interesting models for H diffusion in metals.

Unlike other carbonyl clusters containing heterointerstitial atoms,[6] there is no evidence for rearrangement of the metal skeleton in either the $Rh_{13}$ or $Rh_{14}$ series and this allows a comparison of the electronic properties of the interstitial and surface rhodium atoms which resemble those found for bulk metals.

## Results and Discussion

$[Rh_{13}(CO)_{24}H_n]^{(5-n)-}$ ($n = 1$—4).—A preliminary communication established the ligand fluxionality (CO/H) of the di- and tri-hydride derivatives from their $^1H$, $^1H$-$\{^{103}Rh\}$, and $^{13}C$ n.m.r. spectra at room temperature.[7] Similar measurements have now been carried out on the mono- and tetra-hydride derivatives, together with related low-temperature measurements ($n = 1$—3), and we have also used $^{13}C$-$\{^{103}Rh\}$ and $^{103}Rh$ n.m.r. to make further assignments and obtain additional information.

At room temperature, all the hydride derivatives behave similarly. They all exhibit a complex $^1H$ n.m.r. resonance at high field (see Figure 2 in ref. 7) which is due to both rapid H migration around the *inside* of the hexagonal close-packed cluster and to the exchange of nine of the edge-bridging carbonyls with all twelve terminal carbonyls [Figure 3(*a*)].

At room temperature the $^{13}C$ n.m.r. spectra of all the derivatives consist of a triplet due to three $Rh_B(\mu\text{-}CO)_{hex}Rh_B$ groups and a broad resonance due to exchange of the remaining carbonyls ($CO_{exch}$). This assignment results from the necessity to make all the hexagonal rhodiums ($Rh_B$) equivalent and all the triangular rhodiums ($Rh_C$) equivalent, see later, and is most easily accomplished by a low-energy concerted pseudo-circular pattern of terminal–bridge carbonyl shifts which leads to the conservation of the original distribution of carbonyl ligands [Figure 3(*a*)]. Although this arrangement of carbonyls is not

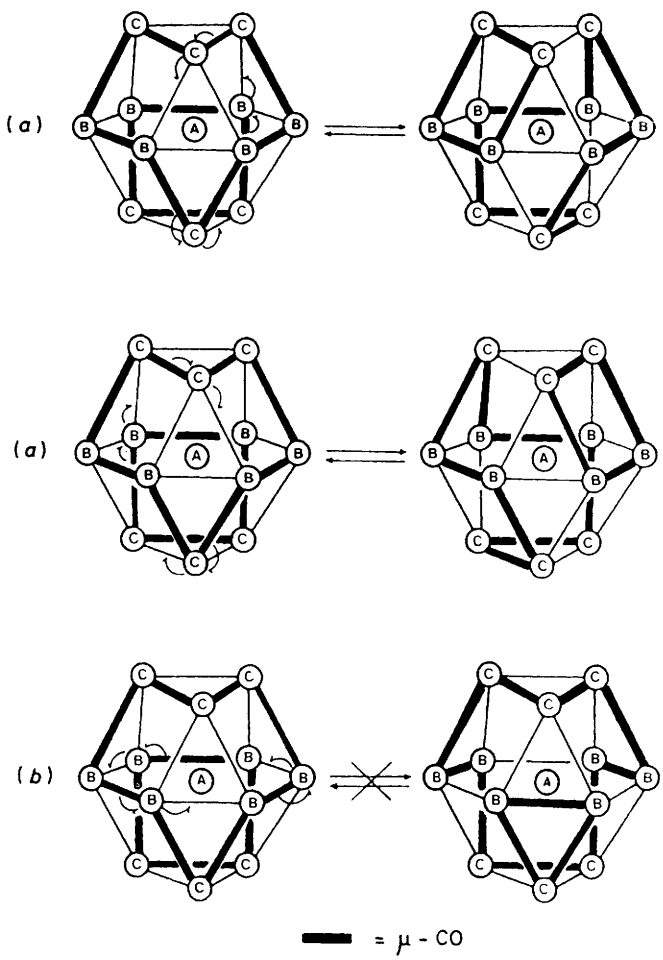


**Figure 3.** (*a*) Carbonyl migrations which conserve the original carbonyl distribution and have the effect of making $Rh^1Rh^2Rh^3Rh^{10}Rh^{11}Rh^{12}$ in Figure 1(*a*) become equivalent ($= Rh_C$) and $Rh^4Rh^5Rh^6Rh^7Rh^8Rh^9$ ($= Rh_B$). Clockwise and anti-clockwise carbonyl migrations, which are not quite equivalent, are possible and both give rise to identical structures. (*b*) Carbonyl migration around the hexagonal $(Rh_B)_6$ plane which does *not* conserve the original carbonyl distribution and variable-temperature n.m.r. measurements suggest does *not* occur at room temperature

unique for hexagonal close-packed metals,[5,8] it seems to be preferred in the $Rh_{13}$ clusters and an alternative step-wise migration of the three edge-bridging and six terminal carbonyls around the hexagonal $Rh_B$ plane would be expected to be of higher energy because it does *not* conserve the original carbonyl distribution [Figure 3(*b*)].

Other work,[9] using the DANTE pulse sequence,[10] has shown that carbonyl fluxionality is more widespread than had been suspected from previous variable-temperature (v.t.) measurements. However, DANTE measurements on $[Rh_{13}(CO)_{24}H_3]^{2-}$ at room temperature do support the conclusions from previous v.t. measurements and show that there is *no* evidence for exchange of $CO_{hex}$ with the remaining carbonyls ($CO_{exch}$).

Room-temperature $^1H$-$\{^{103}Rh\}$ spectra of all the derivatives, except that with $n = 1$, show there to be three resonances due to $Rh_A$, $Rh_B$, and $Rh_C$ [Figure 3(*a*)]; when $n = 1$, it seems probable that $\delta(^{103}Rh_B)$ and $\delta(^{103}Rh_C)$ are coincident. In the other cases, $Rh_B$ and $Rh_C$ have been distinguished by $^{13}C$-$\{^{103}Rh\}$ measurements.

Specific spin decoupling of $Rh_B$ and/or $Rh_C$ allows deconvolution of the room-temperature $^1H$ n.m.r. spectrum, which

**Table 1.** Room-temperature n.m.r. data for $[Rh_{13}(CO)_{24}H_n]^{(5-n)-}$ ($n$ = 1—4) in [$^2H_6$]acetone [see Figure 3(*a*)]

| $n$ | 1 | 2 | 3 | 4 |
|---|---|---|---|---|
| $\delta(^1H)$/p.p.m. | −25.5 | −26.7 | −29.3 | −31.2 |
| $J(^{103}Rh_A–H)$/Hz | 17.1 | 22.3 | 23.2 | 18.6 |
| $J(^{103}Rh_B–H)$/Hz | 5.2 | 5.8 | 5.7 | 4.9 |
| $J(^{103}Rh_C–H)$/Hz | 5.2 | 4.4 | 4.8 | 4.9 |
| $\delta(^{103}Rh_A)$/p.p.m. | +6 370 | +4 954 | +3 547 | +2 917 |
| $\delta(^{103}Rh_B)$/p.p.m. | −340 | −522 | −600 | −527 |
| $\delta(^{103}Rh_C)$/p.p.m. | −340 | −403 | −532 | −536 |
| $\delta(^{13}CO)_{hex}$/p.p.m.[a] | 240.9 | 235.4 | 229.2 | 223.1 |
| $J(^{103}Rh_B–CO_{hex})$/Hz | 39.7 | 38.1 | 38.0 | 39.7 |
| $\delta(^{13}CO)_{exch}$/p.p.m.[b] | 212.3 | 209.8 | 205.5 | 200.7 |

[a] $(CO)_{hex}$ = $Rh_B(\mu\text{-}CO)Rh_B$. [b] $(CO)_{exch}$ = all the carbonyls, except $CO_{hex}$, which are involved in exchange [see Figure 3(*a*)].

can be accurately simulated as a doublet [$J(^{103}Rh_A–H)$] of septets [$J(^{103}Rh_B–H)$] of septets [$J(^{103}Rh_C–H)$].

All the room-temperature n.m.r. data are summarised in Table 1. The magnitude of $J(^{103}Rh_A–H)$ is consistent with a one-bond coupling constant whereas the much smaller couplings to $Rh_B$ and $Rh_C$ are due to time-averaged couplings arising from rapid migration of the hydrogens on the *inside* of the hexagonal close-packed metal skeleton.

Within this closely related series, there are some interesting chemical shift variations which deserve comment. Electron density is withdrawn from the carbonyls to the added protons on successive protonations of $[Rh_{13}(CO)_{24}H]^{4-}$; this results in increased electron density becoming associated with the increasing number of interstitial hydrides. As a result, there is a progressive shift of $\delta(^1H)$ to lower frequency and an analogous shift of $\delta(^{13}CO)$ to lower frequency, with a concomitant increase in ν(CO), because of decreased metal ⟶ carbonyl π bonding. It should also be noted that there is an enormous progressive variation in $\delta(^{103}Rh_A)$ from $n$ = 1—4 whereas $\delta(^{103}Rh_B)$ and $\delta(^{103}Rh_C)$ vary relatively little. The positions of $\delta(^{103}Rh_A)$ and $\delta(^{103}Rh_{B/C})$ are in regions normally associated with positive and low oxidation states respectively.[11] Such a charge differential between surface and interstitial (bulk) metal atoms would be in keeping with related evidence about charge distribution in pure metals,[12–14] and this emerging resemblance in electronic properties between surface metal atoms in carbonyl clusters and bulk metals is reinforced by recent work of Slichter and co-workers.[15] Their solid-state $^{195}Pt$ n.m.r. measurements of CO adsorbed on highly dispersed platinum showed that the values of both $^1J(^{195}Pt–^{13}CO)$ and $\delta(^{195}Pt)$ for surface platinum atoms are very similar to earlier results for $[Pt_n(CO)_{2n}]^{2-}$ ($n$ = 3, 6, 9, or 12)[16] and they conclude that 'clusters are good models for surfaces.'

On decreasing the temperature both carbonyl and hydride mobility decrease but only in the case of $[Rh_{13}(CO)_{24}H_3]^{2-}$ has it been possible to obtain well resolved spectra due to the static structure. It is impossible to go to low temperature for $[Rh_{13}(CO)_{24}H_4]^-$ since solutions always contain excess acid ($CF_3CO_2H$) which freezes at low temperature. For $[Rh_{13}(CO)_{24}H_2]^{3-}$ at −95 °C, two equally intense proton resonances [$\delta(^1H)$ −27.0 and −27.9 p.p.m.] are observed with the resonance at −27.0 p.p.m. being reasonably well resolved, presumably because this is the resonance due to the hydride occupying the $Rh^1Rh^3Rh^4Rh^5$ face [Figure 1(*a*)], see later.

For $[Rh_{13}(CO)_{24}H_3]^{2-}$ at −90 °C, a $^{13}C$ n.m.r. spectrum corresponding to the instantaneous structure is obtained and two proton resonances of intensity 1:2 are observed at −28.2 ($H_A$) and −31.1 p.p.m. ($H_B$) respectively. The resonance at −28.2 p.p.m. is well resolved [Figure 4(*a*)] and consists of a

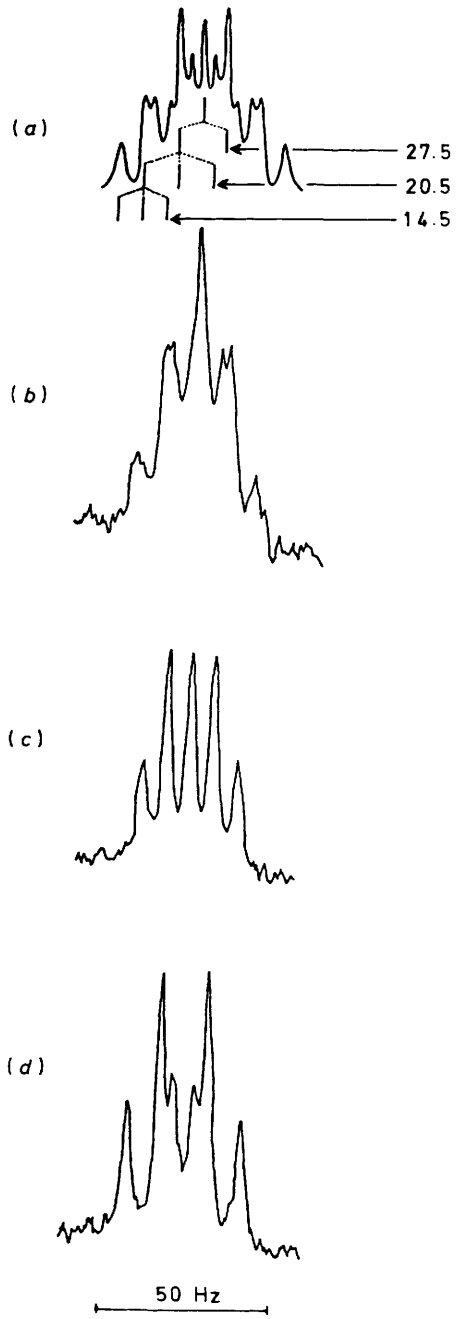


**Figure 4.** The unique $^1H$ n.m.r. resonance ($H_A$) of $[Rh_{13}(CO)_{24}H_3]^{2-}$ at −90 °C. (*a*) Undecoupled, (*b*) $^1H_A$-{$^{103}Rh^{13}$}, (*c*) $^1H_A$-{$^{103}Rh^{1,3}$}, (*d*) $^1H_A$-{$^{103}Rh^{4,5}$}

doublet [$J(^{103}Rh^{13}–H_A)$] of triplets [$J(^{103}Rh^{1,3\text{ or }10,11}–H_A)$] of triplets [$J(^{103}Rh^{4,5}–H_A)$] due to occupancy of one of the two square faces bisected by the plane of symmetry. The occupancy of a hole on the plane of symmetry has been confirmed by specific rhodium decoupling experiments [Figure 4(*b*)—(*d*)] and $^{13}C$-{$^{103}Rh$} measurements, see later, show that it is the square face [$Rh^1Rh^3Rh^4Rh^5$, Figure 1(*a*)] containing only one edge-bridging carbonyl and situated beneath a pentagonal hole on the carbonyl polyhedron that is occupied by hydrogen, rather than the other square face [$Rh^4Rh^5Rh^{10}Rh^{11}$, Figure 1(*a*)], which is surrounded by four edge-bridging carbonyls. Thus, irradiation at either of the relevant peripheral rhodium frequencies [$Rh^{1,3}$ or $Rh^{4,5}$, Figure 1(*a*)] results in the $H_A$

**Table 2.** Low-temperature (−90 °C) $^1$H and $^{103}$Rh n.m.r. data [together with probable assignments: see text and Figure 1(*a*)] for $[N(PPh_3)_2]_2[Rh_{13}(CO)_{24}H_3]$ in $(CD_3)_2CO$

| δ($^1$H)/p.p.m. | δ($^{103}$Rh)/p.p.m.[a] | $^1J(^{103}Rh-^1H)$/Hz | Assignment[b] |
|---|---|---|---|
| −28.2 | +3 578 | 27.5 | $Rh^{13}$–$H_A$ |
| −28.2 | −566 | 19.7 | $Rh^{1,3}$–$H_A$ |
| −28.2 | −730 | 14.2 | $Rh^{4,5}$–$H_A$ |
| −31.1 | +3 578 | 20.2 | $Rh^{13}$–$H_B$ |
| −31.1 | −601 | 16.5 | $Rh^{10,11}$–$H_B$ |
| −31.1 | −649[c] | 14.9 | $Rh^{6,9}$–$H_B$ |
| −31.1 | −644[c] | 7.4 | $Rh^{7,8}$–$H_B$ |
| −31.1 | −1 014 | 13.0 | $Rh^{12}$–$H_B$ |
| | −192 | | $Rh^2$ |

[a] 3.16 MHz = 0 p.p.m. with the $^1$H resonance in $SiMe_4$ being at exactly 100 MHz; shifts to high frequency are positive. [b] See Figure 1(*a*) and text. [c] Assignments could be reversed, see text.

**Table 3.** N.m.r. assignments [see Figure 1(*a*)] for $[Rh_{13}(CO)_{24}H_3]^{2-}$ in [$^2H_6$]acetone at −90 °C ($T_1$ measurements at −78 °C)

| δ($^{13}$CO)/p.p.m. | $^1J(^{103}Rh-^{13}C)$/Hz[a] | $T_1$/s | Carbonyl assignment |
|---|---|---|---|
| 184.9 | 82.0 | | $Rh^{1,3}$ |
| 184.9 | 82.0 | | $Rh^{6,9}$[b] |
| 184.9 | 82.0 | | $Rh^{10,11}$ |
| 185.9 | 78.1 | | $Rh^2$ |
| 186.3 | 89.8 | | $Rh^{4,5}$ |
| 187.1 | 91.8 | | $Rh^{12}$ |
| 188.2 | 88.0 | | $Rh^{7,8}$[b] |
| 228.4 | 36.0 | 1.66 | $Rh^4$–$Rh^5$ |
| 228.9 | 38.0 | 1.51 | $Rh^{6,9}$–$Rh^{7,8}$ |
| 229.9 | 41.0 | 1.24 | $Rh^{4,5}$–$Rh^{10,11}$ |
| 229.9 | 41.0 | 1.24 | $Rh^{7,8}$–$Rh^{12,12}$ |
| 231.7 | 43.0 | 1.13 | $Rh^{1,3}$–$Rh^{2,2}$ |
| 234.4 | 42.0 | 1.09 | $Rh^{10}$–$Rh^{11}$ |
| 236.1 | 41.0 | 1.18 | $Rh^{1,3}$–$Rh^{6,9}$ |

[a] Average value when CO bridges inequivalent nuclei. [b] Assignments could be reversed.

resonance becoming a doublet of triplets whereas decoupling $Rh^{13}$ produces a triplet of triplets.

The broad $H_B$ resonance at −31 p.p.m. can then be attributed to the occupancy of the two equivalent square faces [$Rh^6Rh^7Rh^{11}Rh^{12}$ and $Rh^8Rh^9Rh^{10}Rh^{12}$, Figure 1(*a*)] which each contain two edge-bridging carbonyls and are again situated beneath pentagonal holes on the carbonyl polyhedral surface. Since the four rhodium atoms on these square faces are all inequivalent, it is not surprising that the complicated splitting pattern of this $^1$H resonance is not resolved. However, through decoupling experiments it has been possible to obtain all the values of δ($^{103}$Rh) and $^1J(^{103}Rh-H_B)$. In the static structure, the only rhodium not to be coupled to hydrogen is $Rh^2$ [Figure 1(*a*)] and this chemical shift has been obtained by direct $^{103}$Rh measurements at −90 °C.

The assignment of all these parameters to specific rhodium atoms is more problematical. We have attempted this assignment on the following basis: (*a*) the room-temperature, time-averaged values of $\delta(^{103}Rh_B)$ and $\delta(^{103}Rh_C)$ in Figure 3(*a*) should relate with the statistically weighted value of hexagonal and triangular rhodium chemical shifts in Figure 1(*a*), after allowing for temperature effects, (*b*) the lowest field value of δ($^{103}$Rh) found on decoupling $H_B$ should be associated with $Rh^{12}$ [Figure 1(*a*)] since only this rhodium is common to two hydrides and it is known that δ($^{103}$Rh) shifts to low field for surface rhodium atoms on attachment of hydrogen;[17] our results are shown in Table 2. The $^{103}$Rh shifts then group according to the number of associated hydrides, *viz.* −192 p.p.m. (no hydride), −566 to −730 p.p.m. (one hydride), and −1 014 p.p.m. (two hydrides) and after allowing for temperature effects (*ca.* −0.6 p.p.m. °C$^{-1}$), the weighted average values of the hexagonal [$Rh^{4,5,6,7,8,9}$ in Figure 1(*a*)] and triangular [$Rh^{1,2,3,10,11,12}$ in Figure 1(*a*)] rhodium resonances at −90 °C (−674 and −590 p.p.m. respectively) compare favourably with the observed chemical shifts of $Rh_B$ and $Rh_C$ [Figure 3(*a*)] at room temperature (−600 and −532 p.p.m. respectively).

For the peripheral rhodium atoms, there is a significant variation in the magnitude of $^1J$(Rh–H) and our assignment in Table 2 shows that the largest value is associated with $Rh^{1,3}$. It is therefore tempting to suggest that the hydride ligand is associated more with this *non-carbonyl-bridged* $Rh^1$–$Rh^3$ edge. Applying similar arguments, the lowest value (7.4 Hz) of $^1J(Rh-H_B)$ is assigned to $Rh^{7,8}$, which are associated with *two* bridging carbonyls on the $Rh^6Rh^7Rh^{11}Rh^{12}$/$Rh^8Rh^9Rh^{10}$-$Rh^{12}$ square faces containing $H_B$. Rhodium atoms which are associated with only *one* edge-bridging carbonyl on the square face containing the hydride ligand have intermediate values of $^1J$(Rh–H), *viz.* 13.0—14.9 Hz. Unfortunately, because $^1$H-{$^{103}$Rh} INDOR measurements could not resolve the resonances found directly at −644 and −649 p.p.m. and because of difficulties experienced in obtaining good non-H-decoupled direct $^{103}$Rh n.m.r. spectra in reasonable collection times, it has not been possible unambiguously to relate the two coupling constants (7.4 and 14.9 Hz observed by $^1$H-{$^{103}$Rh} INDOR) to the above resonances (Table 2).

Similarly, at −90 °C a complicated $^{13}$C n.m.r. spectrum is obtained due to the static structure of $[Rh_{13}(CO)_{24}H_3]^{2-}$. On the basis of an extensive series of $^{13}$C-{$^{103}$Rh} double-resonance measurements, we propose the assignments given in Table 3. The average shift of the three edge-bridging carbonyls in the $(Rh_B)_6$ hexagonal plane is 228.7 p.p.m. whilst that of the rest is 205.8 p.p.m. in good agreement with the room-temperature values of $CO_{hex}$ and $CO_{exch}$ (Table 1). The $^{13}$C-{$^{103}$Rh} spectra of the bridging carbonyls were not compatible with the alternative structure in which the hydrides occupy the other set of pseudo-octahedral holes, *i.e.* those with most edge-bridging carbonyl ligands; this is consistent with H occupancy of the three largest pseudo-octahedral metal cavities and expansion of such cavities is obviously facilitated by the absence of bridging carbonyls. The resonance at 188.2 p.p.m. showed a coupling to hydrogen of 15.6 Hz. No similar coupling was resolved on the other $^{13}$C resonances except that $Rh^{12}$–CO (187.1 p.p.m.) appeared to be a poorly resolved triplet [$^2J(H-^{13}C)$ *ca.* 10 Hz]. We cannot determine whether the $^{13}$C resonance at 188.2 p.p.m. is related to $Rh^{6,9}$ or $Rh^{7,8}$ because of the proximity of the $^{103}$Rh signals. However, we suggest that it is $Rh^{7,8}$ since in the solid-state structure[1] this CO group is approximately *trans* to the likely position of $H_B$ which is not true of the CO group on $Rh^{6,9}$ or, indeed, most of the other terminal carbonyl ligands.

It is also interesting that, in agreement with previous $T_1$ measurements on other clusters which have shown that the edge-bridging carbonyl with the fastest $T_1$ has the lowest activation energy for intra-exchange,[18] the resonance attributed to the carbonyls bridging $Rh^4$–$Rh^5$, $Rh^6$–$Rh^7$, and $Rh^8$–$Rh^9$ in $[Rh_{13}(CO)_{24}H_3]^{2-}$ [Figure 1(*a*)] have the longest $T_1$'s (Table 3), consistent with them remaining static.

For the first time in our studies of direct $^{103}$Rh n.m.r., difficulties have been experienced in observing resonances which were detected indirectly by $^1$H-{$^{103}$Rh} INDOR measurements. Thus, direct $^{103}$Rh n.m.r. of $[Rh_{13}(CO)_{24}H_3]^{2-}$ at room temperature clearly showed the interstitial resonance ($Rh_A$) at +3 547 p.p.m. but only *one* other resonance at −600

p.p.m. which corresponds to $Rh_B$ from $^1H$-$\{^{103}Rh\}$ and $^{13}C$-$\{^{103}Rh\}$ measurements. The linewidth of the $Rh_C$ resonance observed by $^1H$-$\{^{103}Rh\}$ INDOR (at a magnetic field of 2.35 T) is much greater than for $Rh_B$ and decreases on raising the temperature from ambient to 50 °C showing that ligand exchange is not fast enough completely to average the widely different $^{103}Rh$ shifts involved (−192 to −1 014 for $Rh_C$ compared to −644 to −730 p.p.m. for $Rh_B$). We estimate the linewidth of $Rh_C$ at a field of 8.4 T to be greater than 500 Hz making direct observation very difficult. Although direct measurements at −90 °C clearly showed the resonance due to the rhodium which is not connected to the static hydrides, $Rh^2$, the resonance of the other single peripheral rhodium, $Rh^{12}$, was too weak to be clearly distinguished had its position not been known from indirect measurements.

From the coalescence temperature (−68 °C) observed in the 200-MHz $^1H$ n.m.r. spectrum of $[Rh_{13}(CO)_{24}H_2]^{3-}$, it is possible to obtain the approximate rate of H exchange (*ca.* 435 $s^{-1}$) and the activation energy for H exchange ($\Delta G‡$ 36.1 kJ $mol^{-1}$). There are large variations in activation energies for H migration in metals[19-22] and this may be related to the jump-distances involved (Table 4). For the hexagonal close-packed $Rh_{13}$ cluster, H migration has to involve octahedral–tetrahedral hole jumps. These distances are similar to those found in cubic close-packed metals which have H diffusion activation energies (*ca.* 21—*ca.* 50 kJ $mol^{-1}$) in a similar range to that found for $[Rh_{13}(CO)_{24}H_2]^{3-}$, whereas H diffusion in body-centred cubic metals is much more facile ($\Delta G‡$ *ca.* 6—21 kJ $mol^{-1}$) due to the possibility of shorter range jumps.

**Table 4.** Interstitial site distances for different metallic structures[a]

| | c.c.p.[b] | b.c.c.[c] | h.c.p.[d] |
|---|---|---|---|
| *d*(oct–oct) | 2*r* | 1.154*r*<br>1.633*r* | 1.633*r* |
| *d*(tet–tet) | 1.414*r* | 0.819*r* | 0.8165*r*<br>1.414*r* |
| *d*(oct–tet) | 1.22*r* | 0.575*r* | 1.225*r*<br>1.32*r* |

[a] *r* = atomic radius. [b] c.c.p. = cubic close-packed. [c] b.c.c. = body-centred cubic. [d] h.c.p. = hexagonal close-packed.

$[Rh_{14}(CO)_{25}H_x]^{(4-x)-}$ ($x$ = 0 or 1).—The *X*-ray structures of $[Rh_{14}(CO)_{25}]^{4-}$[5] and $[Rh_{14}(CO)_{25}H]^{3-}$[4] are very similar and are shown schematically in Figure 2. The low-temperature $^1H$-$\{^{103}Rh\}$ INDOR spectra of the monohydride and $^{13}C$-$\{^{103}Rh\}$ n.m.r. spectra of both derivatives have been reported;[23] these measurements showed that, in both cases, the solid-state metal geometry was retained at low temperatures and that, apart from rapid exchange of terminal/edge-bridging carbonyls around the $(Rh_D)_4$ square face, the distribution and asymmetries of the remaining carbonyls are exactly as found in the solid state. Additionally, $^1H$-$\{^{103}Rh\}$ INDOR measurements on $[Rh_{14}(CO)_{25}H]^{3-}$ showed interstitial H migration to be occurring but, since any perturbation of the complex hydride multiplet resulting from coupling to $Rh_A$ is only small, it was possible to obtain evidence for H coupling to only $Rh_I$, $Rh_B$, $Rh_C$, and $Rh_D$ and *not* $Rh_A$.

We now report direct $^{103}Rh$ n.m.r. measurements and $^{13}C$ n.m.r. spectra on both $Rh_{14}$ compounds at room temperature which show that there is both complete randomisation of carbonyls on the outside of the intact metal skeleton and interstitial H migration within the whole metal skeleton of $[Rh_{14}(CO)_{25}H]^{3-}$ (see Table 5).

All the resonances in the $^{13}C$ n.m.r. spectra of $[Rh_{14}(CO)_{25}H_x]^{(4-x)-}$ ($x$ = 0 or 1), which are well resolved at low temperature (see Figure 2 in ref. 23), simultaneously broaden on increasing the temperature until at room temperature only a single broad resonance is observed at *ca.* 220 and *ca.* 212 p.p.m. for $x$ = 0 and 1 respectively and these chemical shifts compare favourably with the weighted average values of 221.6 and 211.9 p.p.m. obtained from the low-temperature data.

The direct $^{103}Rh$ n.m.r. spectrum of $[Rh_{14}(CO)_{25}]^{4-}$ at room temperature is shown in Figure 5 and clearly shows

**Table 5.** N.m.r. data for $[Rh_{14}(CO)_{25}H_x]^{(4-x)-}$ ($x$ = 0 or 1)

| | $x$ = 0 | | $x$ = 1 | |
|---|---|---|---|---|
| Temp. (°C) | −60 | +25 | −80 | +25 |
| Solvent | EtCN | MeCN–$(CD_3)_2CO$[a] | $(CD_3)_2CO$ | $(CD_3)_2CO$ |
| $\delta(^1H)$/p.p.m. | | | | −31.4 |
| $\delta(^{103}Rh_A)$/p.p.m. | +200 | +230 | +136 | +152 |
| $\delta(^{103}Rh_B)$/p.p.m. | −939 | −895 | −840 | −817 |
| $\delta(^{103}Rh_C)$/p.p.m. | +320 | +375 | +231 | +246 |
| $\delta(^{103}Rh_D)$/p.p.m. | −1 001 | −947 | −973 | −964 |
| $\delta(^{103}Rh_I)$/p.p.m. | *b* | *b* | +5 936 | +5 867 |
| $\delta(^{13}CO_A)$/p.p.m. | 192.7 | | 185.7 | |
| $\delta(^{13}CO_B)$/p.p.m. | 186.2 | | 181.2 | |
| $\delta(^{13}CO_C/^{13}CO_F)$/p.p.m. | 208.5 | *ca.* 220 | 202.0 | *ca.* 212 |
| $\delta(^{13}CO_D)$/p.p.m. | 232.9 | | 219.0 | |
| $\delta(^{13}CO_E)$/p.p.m. | 250.5 | | 237.0 | |
| $^1J(^{103}Rh_A–^{13}CO_A)$/Hz | 102 | | 101 | |
| $^1J(^{103}Rh_C–^{13}CO_B)$/Hz | 89 | | 91.5 | |
| $^1J(^{103}Rh_D–^{13}CO_C/^{13}CO_F)$/Hz[c] | 21.5 | | *d* | |
| $^1J(^{103}Rh_A–^{13}CO_D)$/Hz | 17 | | 15 | |
| $^1J(^{103}Rh_B–^{13}CO_D)$/Hz | 62 | | 61 | |
| $^1J(^{103}Rh_B–^{13}CO_E)$/Hz | 44 | | 44 | |
| $^1J(^{103}Rh_C–^{13}CO_E)$/Hz | 44 | | 37 | |
| $J(^{103}Rh_A–H)$/Hz[c] | | | | 3.7[e] |
| $J(^{103}Rh_C–H)$/Hz[c] | | | | 3.9[e] |
| $J(^{103}Rh_I–H)$/Hz[c] | | | 16.5 | |

[a] 4:1. [b] Not observed. [c] Time-averaged coupling. [d] Not well resolved at this temperature. [e] ±0.4 Hz.

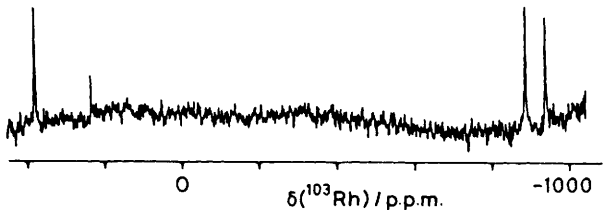


**Figure 5.** Direct $^{103}$Rh n.m.r. spectrum of $[NEt_4]_4[Rh_{14}(CO)_{25}]$ in MeCN–$(CD_3)_2CO$ (4:1) at room temperature

resonances at 375, 230, −895, and −947 p.p.m., which can be assigned to $Rh_C$, $Rh_A$, $Rh_B$, and $Rh_D$ respectively from a comparison with low-temperature $^{13}$C-{$^{103}$Rh} measurements [−60 °C; δ($^{103}$Rh) = 320, 200, −939, and −1 001 p.p.m. for $Rh_C$, $Rh_A$, $Rh_B$, and $Rh_D$ respectively[23]]. Despite $^{103}$Rh being 100% abundant, it is a rather insensitive n.m.r. nucleus and measurement of direct $^{103}$Rh n.m.r. spectra is still not easy even at 11.4 MHz. The spectrum shown in Figure 5 was obtained after 40 000 scans on a solution containing 0.5 g of $[NEt_4]_4[Rh_{14}(CO)_{25}]$ in 5 cm$^3$ of MeCN–$(CD_3)_2CO$ (4:1) in a 15-mm n.m.r. tube but attempts, using the same solution, to locate the interstitial $^{103}Rh_I$ resonance were unsuccessful. This could be attributed to chemical shift anisotropy and/or a small coupling of $Rh_I$ with the peripheral rhodium atoms, which could result in the resonance due to $Rh_I$ being sufficiently broadened with respect to $Rh_A$ as to make it unobservable. Similar problems were found with direct $^{103}$Rh n.m.r. measurements on $[Rh_{14}(CO)_{25}H]^{3-}$. In this case, four peripheral rhodium resonances were clearly observed [δ($^{103}$Rh) = 246, 152, −817, and −964 p.p.m. for $Rh_C$, $Rh_A$, $Rh_B$, and $Rh_D$ respectively] and the non-H-decoupled spectrum showed the resonance due to $Rh_A$ to be a doublet with $J(^{103}Rh_A–H)$ = 3.7 Hz and similar to $J(^{103}Rh_C–H)$ = 3.9 Hz. Despite not being able to detect $Rh_I$ directly, it was located by $^1$H-{$^{103}$Rh} INDOR measurements [δ($^{103}Rh_I$) = +5 867 p.p.m. at room temperature] and H migration thus occurs within the whole metal skeleton which, at room temperature in solution, retains the geometry found in the solid state. This rigidity of the metal skeleton probably stems from the effective close packing made possible by it being homometallic since the metal skeletons encapsulating heterointerstitial atoms are often extremely fluxional.[6]

## Experimental

$^1$H-{$^{103}$Rh} INDOR, $^{13}$C, $^{13}$C-{$^{103}$Rh}, and $^{103}$Rh measurements were made as described previously.[17,24,25] $^2$H N.m.r. measurements were made on a JEOL PS-100 spectrometer using 10-mm n.m.r. tubes. Hydrogen-1 and carbon-13 chemical shifts are referenced to $SiMe_4$ and $^{103}$Rh chemical shifts are referenced to 3.16 MHz (equals 0 p.p.m. at such a magnetic field that the protons in $SiMe_4$ in $CDCl_3$ solution resonate at exactly 100 MHz).

All manipulations were carried out in the absence of air using standard Schlenk-tube techniques. Solvents were purified by standard methods and stored under nitrogen. $[Rh_4(CO)_{12}]$ was prepared as already described.[26] $^{13}$CO-enriched samples of the $Rh_{13}$ and $Rh_{14}$ series were obtained as described below from the pre-enriched $[Rh_{13}(CO)_{24}H_3]^{2-}$ and $[Rh_{15}(CO)_{27}]^{3-}$ anions respectively.

$[Rh_{13}(CO)_{24}H_3]^{2-}$.—$[Rh_4(CO)_{12}]$ (1 g) in propan-2-ol (25 cm$^3$) and water (0.2 cm$^3$) was treated under hydrogen with a solution of NaOH in propan-2-ol (0.1 mol dm$^{-3}$, 8.2 cm$^3$, mol ratio $OH^-$:Rh=2:13). The mixture was vigorously stirred while heating on an oil-bath at 80 °C for 20—24 h. The resulting brown solution was filtered, evaporated to dryness in vacuum, and the residue dissolved in water (10 cm$^3$) under nitrogen. After briefly evacuating (to eliminate the residual traces of propan-2-ol), the solution was treated dropwise, while stirring, with the same volume of an aqueous solution of NaCl (10 g in 100 cm$^3$) to give a crystalline precipitate of the sodium salt which was filtered off, washed with an aqueous solution of NaCl (5 g in 100 cm$^3$ of water) in 5-cm$^3$ portions until the washings were nearly colourless and then vacuum dried. The product contains some NaCl but can be used as such for most purposes. Yields 70—80% based on Rh. Salts of bulky cations were obtained by metathesis in propan-2-ol. $^{13}$CO-enriched samples (*ca.* 30—40%) were obtained *via* direct exchange with $^{13}$CO in tetrahydrofuran (thf) solution for 24 h using standard vacuum line techniques.

$[Rh_{13}(CO)_{24}H_4]^-$.—Solutions of this anion were obtained directly in an n.m.r. tube by addition of $CF_3CO_2H$ (0.25 cm$^3$) to a solution of $[N(PPh_3)_2]_2[Rh_{13}(CO)_{24}H_3]$ (0.15 g) in $CH_2Cl_2$ (2.5 cm$^3$). Protonation of $[N(PPh_3)_2]_2[Rh_{13}(CO)_{24}H_3]$ was confirmed by the expected shift of the i.r. absorptions to higher frequencies ($\nu_{CO}$ 2 040vs, 1 865m cm$^{-1}$).

$[Rh_{13}(CO)_{24}H_2]^{3-}$.—A solution of $Na_2[Rh_{13}(CO)_{24}H_3]$ (0.5 g) in MeOH (20 cm$^3$) was stirred (at least overnight) with anhydrous $Na_2CO_3$ (0.3 g) until the i.r. spectrum showed only the absorption bands of the dihydride at 1 990vs and 1 815m cm$^{-1}$. The solution was filtered and the product precipitated by treatment with a salt containing a bulky cation {$[N(PPh_3)_2]Cl$ or $[PPh_3(CH_2Ph)]Cl$}, filtered off, washed with water, and vacuum dried.

$[Rh_{13}(CO)_{24}H]^{4-}$.—A solution of $Na_2[Rh_{13}(CO)_{24}H_3]$ (0.28 g) in MeCN (12 cm$^3$) was treated dropwise over 1 h with a solution of potassium t-butoxide (0.058 g) in MeCN (12 cm$^3$) (mol ratio 1:3.9). The i.r. spectrum of the final solution shows bands at 1 960vs and 1 780m cm$^{-1}$. The solution was then treated with a solution of $NEt_4Br$ (3 g) in water (30 cm$^3$) and concentrated in vacuum to give a precipitate which was filtered off, washed with propan-2-ol, and vacuum dried. This crude product was purified by extraction with acetone (25 cm$^3$), leaving behind a presently uncharacterised by-product. The filtered acetone solution was concentrated in vacuum to *ca.* 15 cm$^3$, then treated with MeOH (15 cm$^3$), again concentrated to 15 cm$^3$, and addition of another 15 cm$^3$ of MeOH gave a fine crystalline precipitate which was filtered off, washed with MeOH, and vacuum dried.

$[Rh_{15}(CO)_{27}]^{3-}$.—$[Rh_4(CO)_{12}]$ (0.83 g) in propan-2-ol (20 cm$^3$) under nitrogen was treated with a solution of NaOH in propan-2-ol (0.128 mol dm$^{-3}$, 6.9 cm$^3$, mol ratio $OH^-$:Rh=3:15) then refluxed, while stirring, on an oil-bath at 105 °C. After 4 h, the resulting brown solution was evaporated to dryness in vacuum and the residue dissolved in water (20 cm$^3$). After briefly pumping in vacuum to eliminate the last traces of alcohol, the solution was treated with the same volume of an aqueous solution of NaCl (20 g in 100 cm$^3$). After 1 h, the small amount (sometimes there is none) of sodium salts precipitated was filtered off, and the clear solution treated with KBr (15 g) to give a fraction of potassium salts which was filtered, washed with saturated aqueous KBr, and vacuum dried. The desired potassium salt was extracted with acetone (20 cm$^3$) and the solution, after concentration in vacuum to 5 cm$^3$, was treated with bis(2-methoxyethyl) ether (diglyme, dgm) (25 cm$^3$) and concentrated in vacuum until the acetone was eliminated. The resulting crystalline precipitate of the diglyme solvated potassium salt was filtered off, washed with dgm in 5 cm$^3$ portions until the washings were nearly colourless, then with n-hexane and vacuum dried. Should the crystals be sticky, the

crystallisation from acetone–diglyme has to be repeated. Yields 25—35% based on rhodium. The amount of solvated diglyme lies in the range 6—8 mol per mol of $Rh_{15}$.

$^{13}CO$-enriched samples were obtained by direct exchange in acetone for 24 h; the enriched compound was recovered as described above by precipitation with diglyme.

$[Rh_{14}(CO)_{25}]^{4-}$.—A mixture of $K_3[Rh_{15}(CO)_{27}]\cdot n$(dgm) (0.22 g) (described above) with $NEt_4Br$ (0.2 g) was stirred for 1 h in MeCN (10 $cm^3$). The solution was filtered, concentrated in vacuum to *ca.* 4 $cm^3$, and treated dropwise while stirring with propan-2-ol (15 $cm^3$). The crystalline precipitate was filtered off, washed twice with 5 $cm^3$ of propan-2-ol, twice with 2 $cm^3$ of water, again with propan-2-ol and vacuum dried. Yields 80—90% based on rhodium.

$[Rh_{14}(CO)_{25}H]^{3-}$.—A solution of $[NEt_4]_4[Rh_{14}(CO)_{25}]$ (0.44 g) in MeCN (10 $cm^3$) and water (1 $cm^3$) was treated, while stirring, with 1 $cm^3$ of a *ca.* 0.7 mol $dm^{-3}$ solution of phosphoric acid in acetonitrile (prepared by dissolution of 0.5 $cm^3$ of 85% phosphoric acid in 10 $cm^3$ of MeCN). After *ca.* 0.5 h, when only i.r. absorptions due to the hydridic species should be present (see ref. 4), the solution was treated with water (2 $cm^3$) and propan-2-ol (20 $cm^3$) and concentrated in vacuum to *ca.* 10 $cm^3$ to give a precipitate which, after a further addition of 10 $cm^3$ of propan-2-ol was filtered off, washed first with propan-2-ol, then with water, and vacuum dried. Yields 80—90%.

*Deuterium Enrichments.*—Compounds enriched in deuterium were obtained by simple exposure of thf or MeCN solutions containing the hydrides to deuterium for 1—2 d followed by filtration and evaporation to dryness in vacuum.

## Acknowledgements

We thank the S.E.R.C. and C.N.R. for financial support and for high-field n.m.r. facilities. We also thank Dr. I. H. Sadler for carrying out the direct $^{103}Rh$ n.m.r. measurements.

## References

1 V. G. Albano, A. Ceriotti, P. Chini, G. Ciani, S. Martinengo, and W. M. Anker, *J. Chem. Soc., Chem. Commun.*, 1975, 859.
2 V. G. Albano, G. Ciani, S. Martinengo, and A. Sironi, *J. Chem. Soc., Dalton Trans.*, 1979, 978.
3 G. Ciani, A. Sironi, and S. Martinengo, *J. Chem. Soc., Dalton Trans.*, 1981, 519.
4 G. Ciani, A. Sironi, and S. Martinengo, *J. Organomet. Chem.*, 1980, **192**, C42.
5 S. Martinengo, G. Ciani, A. Sironi, and P. Chini, *J. Am. Chem. Soc.*, 1978, **100**, 7096.
6 B. T. Heaton, L. Strona, R. Della Pergola, J. L. Vidal, and R. C. Schoening, *J. Chem. Soc., Dalton Trans.*, 1983, 1941 and refs. therein.
7 S. Martinengo, B. T. Heaton, R. J. Goodfellow, and P. Chini, *J. Chem. Soc., Chem. Commun.*, 1977, 39.
8 A. Fumagalli, S. Martinengo, and G. Ciani, *J. Chem. Soc., Chem. Commun.*, 1984, 1381.
9 B. T. Heaton, E. Occhiello, C. Seregni, and L. Strona, *Organometallics*, submitted for publication.
10 G. A. Morris and R. Freeman, *J. Magn. Reson.*, 1978, **28**, 433.
11 R. J. Goodfellow, in 'N.M.R. and the Periodic Table,' eds. R. K. Harris and B. E. Mann, Academic Press, London, 1978, p. 225.
12 R. H. Citrin, G. K. Wertheim, and Y. Baer, *Phys. Rev. Lett.*, 1978, **41**, 1425.
13 T. M. Duc, O. Guillot, Y. Lassailly, J. Lerante, Y. Jugnet, and J. C. Vedrine, *Phys. Rev. Lett.*, 1979, **43**, 789.
14 J. F. van der Veen, F. J. Himpsel, and D. E. Eastman, *Phys. Rev. Lett.*, 1980, **44**, 189.
15 C. D. Makowka, C. P. Slichter, and J. H. Sinfelt, *Phys. Rev. Lett.*, 1982, **49**, 379.
16 C. Brown, B. T. Heaton, A. D. C. Towl, P. Chini, A. Fumagalli, and G. Longoni, *J. Organomet. Chem.*, 1979, **181**, 233.
17 B. T. Heaton, L. Strona, S. Martinengo, D. Strumolo, R. J. Goodfellow, and I. H. Sadler, *J. Chem. Soc., Dalton Trans.*, 1982, 1499.
18 D. G. Evans, B. T. Heaton, E. Occhiello, and L. Strona, *J. Chem. Soc., Chem. Commun.*, submitted for publication.
19 H. K. Birnbaum and G. Matussiewicz, Second International Congress on Hydrogen in Metals, Paris, June 1977, **1B1**, p. 1.
20 J. H. Wiener, *Phys. Rev. B*, 1976, **14**, 4741.
21 J. Vokl, G. Schaumann, and G. Alefield, *J. Phys. Chem. Solids*, 1970, **31**, 1805.
22 J. Völkl and G. Alefeld, 'Diffusion in Solids,' eds. A. S. Nowick and J. J. Burton, Academic Press, New York, 1975, p. 231.
23 B. T. Heaton, C. Brown, D. O. Smith, L. Strona, R. J. Goodfellow, P. Chini, and S. Martinengo, *J. Am. Chem. Soc.*, 1980, **102**, 6177.
24 G. Longoni, B. T. Heaton, and P. Chini, *J. Chem. Soc., Dalton Trans.*, 1980, 1537.
25 C. Brown, B. T. Heaton, L. Longhetti, W. T. Povey, and D. O. Smith, *J. Organomet. Chem.*, 1980, **192**, 93.
26 S. Martinengo, G. Giordano, and P. Chini, *Inorg. Synth.*, 1980, **20**, 209.

*Received* 8*th August* 1985; *Paper* 5/1383